Iran J Sci Technol Trans Sci (2018) 42:1647–1658
https://doi.org/10.1007/s40995-017-0151-y

RESEARCH PAPER

Analysis of U-shaped NEMS in the Presence of Electrostatic, Casimir, and Centrifugal Forces Using Consistent Couple Stress Theory

Maryam Keivani[1] · Javad Mokhtari[2] · Naeime Abadian[2] · Masoud Abbasi[2,3] · Ali Koochi[4] · Mohamadreza Abadyan[4]

Received: 6 August 2016 / Accepted: 3 January 2017 / Published online: 7 February 2017

Abstract A mathematical model is used to study the effects of the electrostatic, Casimir and centrifugal forces on the static behaviors of the two U-shaped NEMS with rectangular and circular geometries. The size-dependent equations are obtained by employing the consistent couple stress theory (CCST). The D'Alembert principle is used to transform the angular speed into an equivalent static centrifugal force. The equivalent boundary condition technique is applied for obtaining the governing equation of the U-shape actuator. The nonlinear equations are solved by two different approaches, i.e., using a distributed parameter model (in conjunction with Rayleigh–Ritz solution method) and a lumped parameter model. The model is validated by comparing the obtained results with those of experiment as well as finite element simulation. The effect of various parameters on the instability threshold and characteristics of the system is discussed. The obtained results are beneficial for design and fabrication of U-shaped sensors.

Keywords U-shaped NEMS · Centrifugal force · Consistent couple stress theory · Casimir attraction

✉ Masoud Abbasi
masoud_abbasi@shirazu.ac.ir

Naeime Abadian
abadiannaeime@yahoo.com

[1] Shahrekord University of Medical Sciences, Shahrekord, Iran

[2] Department of Mathematics, Isfahan (Khorasgan) BranchIslamic Azad University, Isfahan, Iran

[3] School of Mechanical Engineering, Shiraz University, Shiraz, Iran

[4] Shahrekord Branch, Islamic Azad University, Shahrekord, Iran

1 Introduction

Beam-type micro/nano-electromechanical systems (MEMS/NEMS) are used in various engineering and science categories, i.e., mechanics, chemistry, optics, biology, photonics, electronics, sensing, etc. These systems are increasingly employed in innovating new nano-devices such as actuators, resonators, robots, biosensors, actuators, accelerometer, and tweezers. (Ke and Espinosa 2006; Keivani et al. 2016a). The pull-in instability analysis of miniature actuators is carried out in many studies for reliable design, fabrication and operation of these devices (Rezazadeh et al. 2015; Zhu 2010; Lin and Zhao 2008; Keivani et al. 2016a, b, c, d, e; Mouloodi et al. 2014; Farrokhabadi et al. 2015). The present work is devoted to study the pull-in behavior of the U-shaped NEMS. Recently, some studies have been conducted on the limitations and potentials of using U-shaped MEMS/NEMS (Latorre et al. 1999; Yan et al. 2004; Latorre et al. 1999; Yan et al. 2004; Qian et al. 2012; Koukharenko et al. 2006; Keivani et al. 2016d; Lee 2007; Kopka et al. 2000; Keplinger et al. 2005). Qian et al. studied performance of the U-shaped NEMS consisted of a capacitive rigid plate supported by two silicon nanowires (Qian et al. 2012). The U-shaped actuator for capacitive applications with adjustable tuning range is studied by Yan and coworkers (Yan et al. 2004). They showed that U-shaped structures provide enhanced electrical performance. Koukharenko et al. applied ANSYS software and surveyed the mechanical characteristics of the silicon U-shaped micro-generator (Koukharenko et al. 2006). Keivani et al. investigated the impacts of the vdW force and centrifugal force on the static behavior of the U-shaped and double sided nano-actuators (Keivani et al. 2016d). They applied the modified couple-stress theory (MCST) for deriving the

governing equations and demonstrated that the vdW force decreases the external pull-in voltage of the system.

MEMS/NEMS capacitive sensors are progressively used in modern measurement systems. These devices can be used in fault detection of roller bearing (Renaudin et al. 2010), balancing power plant rotating equipment (Lebold et al. 2004), measurement of high-speed spindle errors in CNC (Jywe and Chen 2005), centrifuge devices for separating the solids form liquids (Huang et al. 2009), and angular speed detection of turbomachinery. In addition, calculating the angular speed is very crucial in rotary systems, working machines, and industrial control systems (Bodson et al. 1995). In the above mentioned applications, the presence of centrifugal force (the outward pressure on an object rotating around a central point) can significantly change the electromechanical response of the NEMS sensors. It is worth mentioning that, the U-shaped sensors have been considered as potential capacitive angular speed sensors and accelerometers (Hou et al. 2010; Azimloo et al. 2014; Shah-Mohammadi-Azar et al. 2013). In this paper, the impact of centrifugal force due to angular velocity on the pull-in behavior of the U-shaped sensors is investigated. The Casimir force (vacuum fluctuations) affects the pull-in behavior of NEMS at the nano-scale separations. Many researchers have been studied the effect of Casimir force on the pull-in instability of NEMSs (Lin and Zhao 2005; Mokhtari et al. 2015; Farrokhabadi et al. 2015; Keivani et al. 2016b; Abdi et al. 2011). Herein, the effect of Casimir force is incorporated in theoretical modeling of the U-shaped NEMS.

Besides the Casimir force, the size dependency is another small-scale phenomenon that might affect the performance of NEMSs, hence should be incorporated in theoretical models. Experiments demonstrate a hardening trend in mechanical characteristic of conductive metals as the dimension reduces to sub-micron (Lam et al. 2003; McFarland and Colton 2005). The classical continuum theory cannot incorporate the size dependency in the constitutive equations. So, the non-classical theories, such as non-local elasticity (Eringen and Edelen 1972), couple-stress theory (Ejike 1969), strain gradient theory (Lam et al. 2003), modified couple-stress theory (Yang et al. 2002), and consistent couple stress theory (Hadjesfandiari and Dargush 2011), have been used to consider the size effect in theoretical continuum models. According to the modified couple stress theory, which has been employed by many researchers to investigate miniature structures (Mokhtari et al. 2015; Baghani 2012; Zhang and Fu 2012), the materials are in equilibrium if the applied forces, classical couples, and moments of couples equal zero. The last premise is just an assumption and was not considered in the classical elasticity theories. Although the theory predicts stiffer models of micro/nanostructures, its correctness is still under question. So, some researchers tried to find another more reasonable solution for this problem. Recently, Hadjesfandiari and Dargush dominate over this issue by using true continuum kinematical displacement and rotation (Hadjesfandiari and Dargush 2011). They showed that the body force and body couple are not distinguishable from each other and the body couple transforms to the equivalent body force (Hadjesfandiari and Dargush 2011; Fakhrabadi and Yang 2015).

This work demonstrates the impact of Casimir force and size phenomenon on the electromechanical instability of U-shaped NEMS in the presence of the centrifugal force. The size effect is modeled using the consistent couple stress theory. The nonlinear governing equations of the nanostructures are derived. The Rayleigh–Ritz method (RRM), and lumped parameter model (LPM) are applied to solve the nonlinear equations.

2 Theory

Figure 1a, b show the schematic view of typical NEMS consist of a conductive movable U-shaped element suspended over a fixed plane electrode. The U-shaped element constructed from two cantilever nanobeams or nanowires stick to a rectangular plate. The DC voltage difference and initial gap between the U-shaped element and the fixed electrode are V and D, respectively. The length, width, and thickness of nano-beam are L, h, and t, respectively. Similarly, the nano-wire length is L and its radius is r

The free-body diagram of the beam/wire cross-section is shown in Fig. 1c that represents the internal structural resultants; in this figure, F and M indicate the force and moment at the free end of the nanobeam/wire ($x = L$), respectively.

2.1 Fundamentals of Consistent Couple Stress Theory

In the CCST, the equilibrium of the linear isotropic materials are formulated as the following (Hadjesfandiari and Dargush 2011):

$$\sigma_{ij,j} + F_i = 0 \tag{1a}$$

$$\mu_{ji,i} + e_{ijk}\sigma_{jk} + C_i = 0 \tag{1b}$$

where e_{ijk}, σ_{ij} and μ_{ij} are the permutation tensor, force-stress tensor (classical), and couple stress tensors. In addition, Fi represent the body force per unit volume of the body and Ci is the body couple per unit volume of the body.

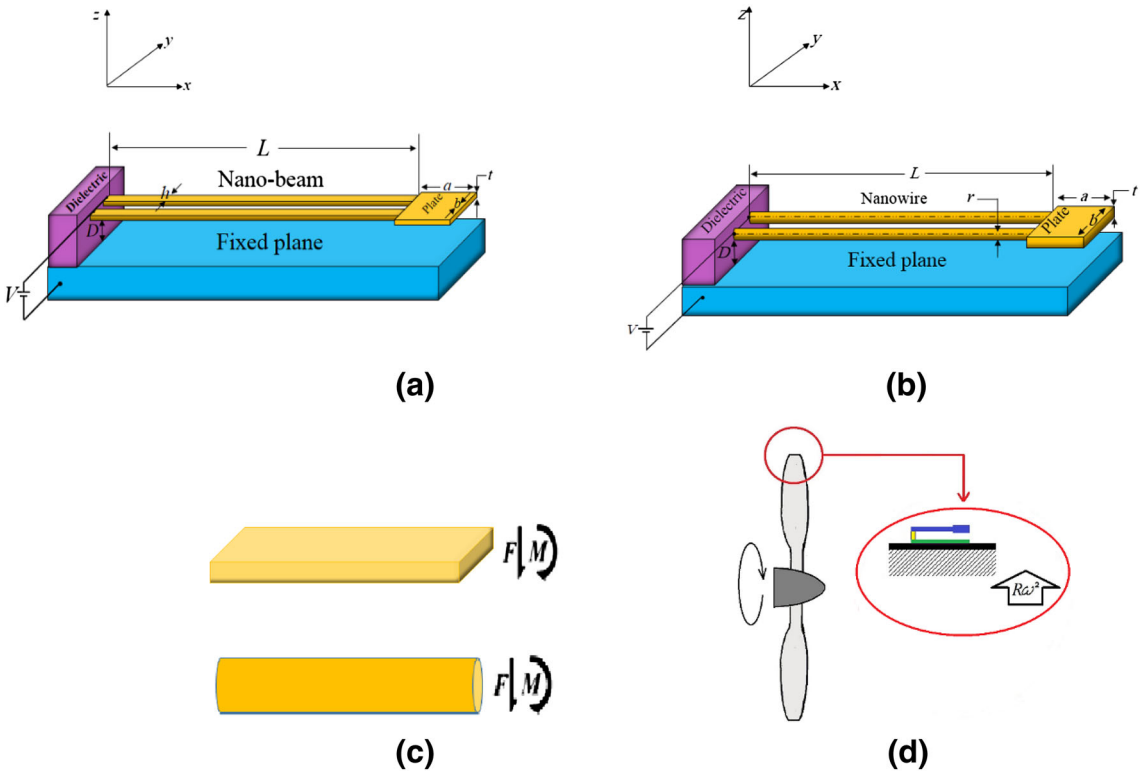

Fig. 1 The schematic representation of **a** U-shaped NEMS made of nanobeam, **b** U-shaped NEMS made of nanowire, **c** internal resultants in arbitrary cross-section, **d** NEMS structure under the presents of centrifugal force

Based on the CCST, the stress tensor is generally non-symmetric. So, it can be decomposed to the symmetric and skew-symmetric components.

$$\sigma_{ij} = \sigma_{(ij)} + \sigma_{[ij]} \tag{2}$$

where $\sigma_{(ij)}$ is the symmetric part and $\sigma_{[ij]}$ is the skew-symmetric part of the force-stress tensor.

Hadjesfandiari and Dargush demonstrated that the couple stress for the isotropic linear materials can be defined as the following (Hadjesfandiari and Dargush 2011)

$$m_i = -8\eta k_i. \tag{3}$$

The above equation demonstrates that the CCST for the isotropic linear materials has only one extra size-dependent parameter. The ratio is the constant and makes difference between the classical and the CCST. For the zero value of size-dependent parameter, l, the latter reduces to the former. Furthermore, Hadjesfandiari and Dargush (2011) proved that the skew-symmetric component of the stress tensor can be written as the following:

$$\sigma_{[ij]} = -m_{[i,j]} \tag{4}$$

Therefore, the strain energy density can be defined as the following (see Keivani et al. 2016c for more information):

$$\bar{U} = \frac{1}{2}\left(\sigma_{(ij)}\varepsilon_{ij} + \mu_{ij}\kappa_{ij}\right) \tag{5}$$

2.2 Nonlinear Governing Equation

The governing equation of the system can be derived from the total energy of one of the beam/wire elements. The total energy includes the strain energy, work done by external forces, internal resultants, and centrifugal force.

2.2.1 Strain Energy of the Beam/Wire

For an Euler–Bernoulli beam/wire, the displacement field can be expressed as:

$$u_1 = -Z\frac{\partial w}{\partial X}, \quad u_2 = 0, \quad u_3 = w \tag{6}$$

where w is the centerline deflection of the beam/wire in the z direction and u_1, u_2, and u_3 are the displacement components in the X, Y, and Z directions, respectively.

By considering small deformation, and substituting the displacement field of the Euler–Bernoulli beam/wire and applying Eq. (3) one can obtains (see Keivani et al. 2016c for more information):

$$\kappa_{XY} = \kappa_{YX} = -\frac{1}{2}\frac{\partial^2 w}{\partial X^2}, \quad \kappa_{XX} = \kappa_{YY} = \kappa_{ZZ} = \kappa_{YZ} = \kappa_{ZY} = \kappa_{ZX} = \kappa_{XZ} = 0 \tag{7a}$$

$$\mu_{XY} = -\mu_{YX} = 4\mu l^2 \frac{\partial^2 w}{\partial X^2}, \quad \mu_{XX} = \mu_{YY} = \mu_{ZZ} = \mu_{YZ} = \mu_{ZY} = \mu_{ZX} = \mu_{XZ} = 0 \tag{7b}$$

$$\varepsilon_{XX} = -Z\frac{\partial^2 w}{\partial X^2}, \quad \varepsilon_{ZZ} = \varepsilon_{YY} = \varepsilon_{XY} = \varepsilon_{YZ} = \varepsilon_{ZX} = 0 \tag{7c}$$

$$\sigma_{XX} = -EZ\frac{\partial^2 w}{\partial X^2}, \quad \sigma_{ZZ} = \sigma_{YY} = \sigma_{XY} = \sigma_{YZ} = \sigma_{ZX} = 0 \tag{7d}$$

By substituting Eq. (7) in Eq. (5) after some elaborations and integrating over the beam/wire volume, the bending strain energy is obtained as the following:

$$\begin{aligned} U =& \frac{1}{2}\int_0^L \int_A \left\{ 4\mu l^2 \frac{\partial^2 w}{\partial X^2}\left(\frac{1}{2}\frac{\partial^2 w}{\partial X^2}\right) - 4\mu l^2 \frac{\partial^2 w}{\partial X^2}\left(-\frac{1}{2}\frac{\partial^2 w}{\partial X^2}\right) \right. \\ & \left. -z\frac{\partial^2 w}{\partial X^2}\left(-zE\frac{\partial^2 w}{\partial X^2}\right)\right\} \mathrm{d}A\mathrm{d}X \\ =& \frac{1}{2}\int_0^L \left[(EI + 4\mu A l^2)\left(\frac{\partial^2 w}{\partial X^2}\right)^2 \right] \mathrm{d}X \end{aligned} \tag{8}$$

2.2.2 Work Done by External Forces

For each beam/wire element, the work done by external forces, $V_{f_{\text{ext}}}$, can be determined as

$$V_{f_{\text{ext}}} = \int_0^L \int_0^w f_{\text{ext}} \mathrm{d}w\mathrm{d}X \tag{9}$$

where the external forces, f_{ext}, (9) is the summation of the electrostatic and Casimir forces per unit length of the beam/wire.

The electrostatic force in relation (9) can be determined from the capacitive model (Jackson 1998). Based on capacitive model, the electrical attraction per unit length of the beam, f_{elec}, in the case of nanobeam is expressed as (Gupta 1997):

$$f_{elec} = \frac{\varepsilon_0\, \varepsilon_r h V^2}{2D^2}\left(1 + 0.65\frac{D}{h}\right), \tag{10}$$

where ε_0, ε_r, h, D, and V are the permittivity of vacuum, dielectric constant, the beam width, the gap distance, and the applied voltage, respectively. According to parallel plate model, the Casimir force per unit length f_{Cas}, is derived by differentiating the energy as (2015)

$$f_{\text{Cas}} = \frac{\pi^2 \overline{h} c h}{240 D^4}, \tag{11}$$

where $\overline{h} = 1.05457 \times 10^{-34}$ J.s is the reduced Planck's constant and $c = 2.998 \times 108$ m/s is the speed of light.

Similarly, for the U-shaped element made of nanowire (Fig. 1b), the electrostatic force in relation (9) can be determined from the capacitive model as the following (Hayt 1981):

$$f_{\text{elec}} = \frac{\pi \varepsilon_0 \varepsilon_r V^2}{\sqrt{(D+2r)(D)}\,\text{arccosh}^2\left(1+\frac{D}{r}\right)} \tag{12}$$

where r is radius of the nanowire.

A simplistic approach for determining the vacuum fluctuations among complex bodies is the proximity force approximation (PFA). Based on the PFA, the interacting systems with complex geometries are considered as summation of infinitesimal parallel surfaces (Bordag et al. 2001; Emig et al. 2006). Based on the PFA, the Casimir force for a conductive cylinder parallel to a conductive plane is determined by differentiating the energy as (Bordag et al. 2001; Emig et al. 2006)

$$f_{\text{Cas}} = \frac{\pi^3 \bar{h} c}{768}\sqrt{\frac{2r}{D^7}}. \tag{13}$$

Finally, f_{ext} can be defined by summation of the electrostatic and Casimir forces and replacing D with $D - w$ in relations (10)–(13) as:

$$f_{\text{ext}} = f_{\text{elec}} + f_{\text{Cas}} = \begin{cases} \dfrac{\varepsilon_0\, \varepsilon_r h V^2}{2(D-w)^2}\left(1 + 0.65\dfrac{(D-w)}{h}\right) + \dfrac{\pi^2 \overline{h} c h}{240(D-w)^4} & \text{nanobeam} \\ \dfrac{\pi \varepsilon_0 \varepsilon_r V^2}{\sqrt{(D-w+2r)(D-w)}\,\arccos h^2\left(1+\dfrac{D-w}{r}\right)} + \dfrac{\pi^3 \bar{h} c}{768}\sqrt{\dfrac{2r}{(D-w)^7}}. & \text{nanowire} \end{cases} \tag{14}$$

2.2.3 Work Done by Centrifugal Force

According to D'Alembert principle, one can transform an angular speed into an equivalent centrifugal force. Hence, the contribution of the centrifugal force can be modeled by considering the angular velocity of the system. The centrifugal force per unit length of the nanobeam, caused by rotation of a rotary machine, is determined as (Azimloo et al. 2014; Shah-Mohammadi-Azar et al. 2013)

$$f_{Rot} = \rho ht(R \pm D)\omega^2, \tag{15}$$

where ρ, R, and ω are the density of the nanobeam, the rotary surface radius, and the angular speed of the rotary surface, respectively. For the case of $R \gg D$, Eq. (15) reduces to

$$f_{\mathrm{Rot}} = \rho htR\omega^2. \tag{16}$$

Similarly, the centrifugal force per unit length of the nanowire, caused by rotation of a rotary machine, is determined as (Azimloo et al. 2014; Shah-Mohammadi-Azar et al. 2013)

$$f_{\mathrm{Rot}} = \pi\rho r^2 R\omega^2. \tag{17}$$

Now, the work done by centrifugal force for each wire/beam element, $V_{f_{\mathrm{Rot}}}$, can be determined as

$$V_{f_{\mathrm{Rot}}} = \int_0^L \int_0^w f_{\mathrm{Rot}} \mathrm{d}w\mathrm{d}X \tag{18}$$

2.2.4 Work Done by Beam/Wire Tip Resultants

For the U-shaped system, the stress resultants F and M are induced by the electrostatic and Casimir attractions between the rigid plate and the ground as well as the angular speed. The work done by the moment traction, VM, is obtained as:

$$V_M = \int_0^{\frac{\partial w(L)}{\partial X}} M\left(w(L), \frac{\partial w(L)}{\partial X}\right) \times \mathrm{d}\frac{\partial w(L)}{\partial X} \tag{19}$$

The work done by the force traction, VF, is determined as:

$$V_F = \int_0^{w(L)} F\left(w(L), \frac{\partial w(L)}{\partial X}\right) \times \mathrm{d}w(L) \tag{20}$$

ters are defined asated asdTo obtain appropriate expression for F and M, the distributed forces act on the plate are replaced with an equivalent concentrated force acts at the distance of $\bar{x}$ from the beam/wire tip (the force center). The value of $\bar{x}$ is determined from $\bar{x} = M/F$ relation. Using numerical computations, it is found that for any geometry, the value of $\bar{x}$ is approximately constant for wide ranges of the deflection and slope values ($\bar{x} = 0.5a \sim 0.52a$). The overall error of the simplification is less than 1% which is in the acceptable range.

The force $\bar{F}$ and moment $\bar{M}$ are the summation of the force and moment due to electrostatic, Casimir and centrifugal forces. For a typical rigid plate with length of a, and width of b, the force resultant (summation of the electrostatic, Casimir and centrifugal forces) can be approximated as:

$$\begin{aligned}\bar{F} &= F_{\mathrm{elec}} + F_{\mathrm{Cas}} + F_{\mathrm{Rot}} \\ &= \frac{\varepsilon_0\varepsilon_r}{2}\frac{abV^2}{(D - w(L) - \bar{x}w'(L))^2} \\ &\quad + \frac{\pi^2\hbar cab}{240(D - w(L) - \bar{x}w'(L))^4} + \rho abtR\omega^2\end{aligned} \tag{21}$$

and the moment resultant is approximated as

$$\begin{aligned}\bar{M} &= \mathrm{M}_{\mathrm{elec}} + \mathrm{M}_{\mathrm{Cas}} + \mathrm{M}_{\mathrm{Rot}} \\ &= \frac{\varepsilon_0\varepsilon_r}{2}\frac{abV^2\bar{x}}{(D - w(L) - \bar{x}w'(L))^2} \\ &\quad + \frac{\pi^2\hbar cab\bar{x}}{240(D - w(L) - \bar{x}w'(L))^4} + \frac{\rho a^2 btR\omega^2}{2}\end{aligned} \tag{22}$$

The above relations describe the total forces and moments induced by the tip-plate. It should be noted that half of the forces and momentum resultants should be considered as the contribution of each beam/wire.

2.2.5 Total Energy of the Beam/Wire

The total energy of the beam/wire can be summarized as:

$$\begin{aligned}\Pi = &-\frac{1}{2}\int_0^L \left[(EI + 4\mu Al^2)\left(\frac{\partial^2 w}{\partial X^2}\right)^2\right]\mathrm{d}X \\ &+ \int_0^L \int_0^W f_{\mathrm{ext}}(X)\mathrm{d}W\mathrm{d}X + \int_0^{\frac{\partial w(L)}{\partial X}} M\left(w(L), \frac{\partial w(L)}{\partial X}\right)\mathrm{d}\frac{\partial w(L)}{\partial X} \\ &+ \int_0^{w(L)} F\left(w(L), \frac{\partial w(L)}{\partial X}\right)\mathrm{d}w(L)\end{aligned} \tag{23}$$

Now, by substituting Eqs. (14), (16), (17), (21), and (22) in Eq. (23), considering some mathematical elaborations the dimensionless total energy can be explained as:

$$\bar{\Pi} = \frac{1}{2}\int_0^1 \left[(1+\delta)\left(\frac{\partial^2 \hat{w}}{\partial x^2}\right)^2\right]\mathrm{d}x - \int_0^1\int_0^w (\bar{F})\mathrm{d}w\mathrm{d}x + \int_0^{\hat{w}(1)} \vartheta[\bar{P}+\bar{\omega}]\mathrm{d}\hat{w} - \int_0^{\hat{w}'(1)} \vartheta\Omega\xi\tau\left[\bar{P}+\frac{\bar{\omega}}{2\Omega}\right]\mathrm{d}\hat{w}' \tag{24}$$

where

$$\bar{F} = \begin{cases} \beta\left[\dfrac{1}{(1-\hat{w})^2} + 0.65\dfrac{k}{(1-\hat{w})}\right] + \dfrac{\gamma}{(1-\hat{w})^4} + \bar{\omega} & \text{nanobeam} \\ \dfrac{2k^{\frac{3}{2}}\beta}{\sqrt{(1-\hat{w})[1+\bar{k}(1-\hat{w})]}\arccos h^2(1+2\bar{k}(1-\hat{w}))} + \dfrac{5k^{\frac{1}{2}}\gamma}{16(1-\hat{w})^{\frac{7}{2}}} + \dfrac{\bar{\omega}}{4} & \text{nanowire} \end{cases} \tag{25a}$$

$$\bar{P} = \frac{\beta}{(1-\hat{w}(1)-\Omega\xi\tau\hat{w}'(1))^2} + \frac{\gamma}{(1-\hat{w}(1)-\Omega\xi\tau\hat{w}'(1))^4} \tag{25b}$$

In Eqs. (24) and (25), the dimensionless parameters are defined as:

$$x = \frac{X}{L},\quad \hat{w} = \frac{w}{D},\quad \xi = \frac{a}{D},\quad \tau = \frac{D}{L},$$

$$k = \begin{cases} \dfrac{D}{h} & \text{nanobeam} \\ \dfrac{D}{2r} & \text{nanowire} \end{cases},\quad \delta = \frac{\mu A l^2}{E_{eff} I},$$

$$\vartheta = \begin{cases} \dfrac{ab}{2hL} & \text{nanobeam} \\ \dfrac{ab}{4\pi rL} & \text{nanowire} \end{cases},\quad \Omega = \frac{\bar{x}}{a},$$

$$\gamma = \begin{cases} \dfrac{\pi^2 \bar{h} c h L^4}{240 E_{\text{eff}} I D^5} & \text{nanobeam} \\ \dfrac{\pi^3 \bar{h} c r L^4}{120 E_{eff} I D^5} & \text{nanowire} \end{cases}, \tag{26}$$

$$\beta = \begin{cases} \dfrac{\varepsilon_0 \varepsilon_r V^2 h L^4}{2 E_{\text{eff}} I D^3} & \text{nanobeam} \\ \dfrac{\varepsilon_0 \varepsilon_r \pi r V^2 L^4}{E_{e\text{eff}} I D^3} & \text{nanowire} \end{cases},$$

$$\bar{\omega} = \begin{cases} \dfrac{\rho h t R \omega^2 L^4}{E_{\text{eff}} I D} & \text{nanobeam} \\ \dfrac{2\pi r \rho t R \omega^2 L^4}{E_{\text{eff}} I D} & \text{nanowire} \end{cases},$$

3 Solving Methods

3.1 Rayleigh–Ritz Method

To employ the Rayleigh–Ritz method the displacement is expressed as a combination of a complete set of independent basis functions $\varphi_i(x)$ in the form of:

$$\hat{w}(x) = \sum_{i=1}^{n} q_i \phi_i(x) \tag{27}$$

where the index i refers to the number of modes included in the simulation. The classical mode shapes of cantilever nanobeam are used in the Rayleigh–Ritz method.

$$\phi_i(\xi) = \cosh(\omega_i\xi) - \cos(\omega_i\xi) - \frac{\cosh(\omega_i) - \cos(\omega_i)}{\sinh(\omega_i) - \sin(\omega_i)}(\sinh(\omega_i\xi) - \sin(\omega_i\xi)) \tag{28}$$

where ω_i is the ith root of characteristic equation of the cantilever beams based on the the classical theory. Minimizing the total energy implies that:

$$\frac{\partial \bar{\Pi}}{\partial q_i} = 0 \quad i = 0, 1, \ldots, N \tag{29}$$

Substituting (24) and (27) into (29), assuming the orthogonality of $\varphi_i(x)$ and then following some straightforward mathematical operations, a system of governing equations can be fined as:

$$[1+\delta]\omega_i^4 q_i - \int_0^1 \phi_i(\bar{F}_R + +\bar{\omega})\mathrm{d}x - \vartheta[\bar{P}_R + \bar{\omega}]\phi_i|_{x=1} - \vartheta\Omega\xi\tau\left[\bar{P}_R + \frac{\bar{\omega}}{2\Omega}\right]\phi_i'\Big|_{x=1} = 0 \quad i = 1, 2, \ldots, N \tag{30}$$

where:

$$\bar{F}_R = \begin{cases} \beta\left[\dfrac{1}{\left(1-\sum_{j=1}^{N} q_j\phi_j\right)^2} + 0.65\dfrac{k}{\left(1-\sum_{j=1}^{N} q_j\phi_j\right)}\right] + \dfrac{\gamma}{\left(1-\sum_{j=1}^{N} q_j\phi_j\right)^4} + \bar{\omega} & \text{nanobeam} \\ \dfrac{2k^{\frac{3}{2}}\beta}{\sqrt{\left(1-\sum_{j=1}^{N} q_j\phi_j\right)\left[1+\bar{k}\left(1-\sum_{j=1}^{N} q_j\phi_j\right)\right]}\operatorname{arccosh}^2\left(1+2\bar{k}\left(1-\sum_{j=1}^{N} q_j\phi_j\right)\right)} + \dfrac{5k^{\frac{1}{2}}\gamma}{16\left(1-\sum_{j=1}^{N} q_j\phi_j\right)^{\frac{7}{2}}} + \dfrac{\bar{\omega}}{4} & \text{nanowire} \end{cases} \tag{31a}$$

$$\bar{P}_R = \frac{\beta}{\left(1-\sum_{j=1}^{N} q_j\phi_j - \Omega\xi\tau\sum_{j=1}^{N} q_j\phi_j'\right)^2} + \frac{\gamma}{\left(1-\sum_{j=1}^{N} q_j\phi_j - \Omega\xi\tau\sum_{j=1}^{N} q_j\phi_j'\right)^4} \tag{31b}$$

Finally, the MAPLE commercial software is employed to solve the system of equations numerically.

3.2 Lumped Parameter Model (LPM)

The LPM assumes uniform force distribution along the beam length (Lin and Zhao 2005) as shown in Fig. 2.

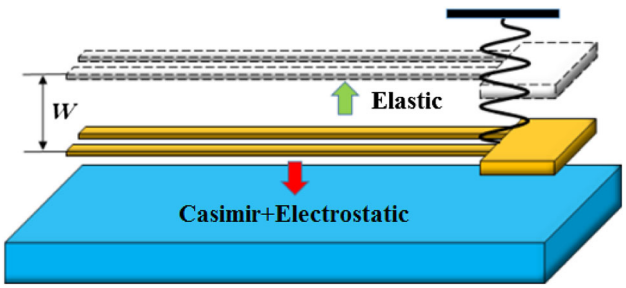

Fig. 2 The schematic configuration of LPM of U-shaped sensors

The mechanical response of the beam/wire is expressed by a linear elastic spring

$$Kw_{\text{tip}} = f \tag{32}$$

where f is the total force acting on the beam/wire.

For U-shaped device, the total deflection is the summation of three values, i.e., the deflection of the beam subjected to (a) uniform load of f_{ext} and f_{Rot} along the beam/wire, (b) a force of F at the free end, and (c) a moment of M at the free end. These three deflections can be determined by superposition of three serial springs with the spring constants of K_1, K_2, and K_3, respectively. Hence, the elastic stiffness of the U-shaped sensor can be determined as:

$$\begin{aligned} K &= \left[\frac{1}{K_1}+\frac{1}{K_2}+\frac{1}{K_3}\right]^{-1} \\ &= \left[\left(\frac{8(E_{\text{eff}}I+4\mu Al^2)}{L^3}\right)^{-1} + \left(\frac{6f(E_{\text{eff}}I+4\mu Al^2)}{FL^2}\right)^{-1} \right. \\ &\quad \left. + \left(\frac{4f(E_{\text{eff}}I+4\mu Al^2)}{ML}\right)^{-1}\right]^{-1} = \frac{24f(E_{\text{eff}}I+4\mu Al^2)}{3fL^3+4FL^2+6ML} \end{aligned} \tag{33}$$

By substituting the stiffness (Eq. (33) and the force terms in (32), the governing equations of the nanostructures are easily obtained. Finally, using the dimensionless relations (26), the relation between the nondimensional deflection, w_{tip}, and the nondimensional voltage, β, is obtained as

$$\beta = \begin{cases} \dfrac{24\hat{w}_{\text{tip}}(1+\delta) - \dfrac{8\gamma\vartheta+12\vartheta\gamma\Omega\xi\tau}{(1-\hat{w}_{\text{tip}})^4} - \dfrac{3\gamma}{(1-\hat{w}_{\text{tip}})^4} - (3+8\vartheta+12\vartheta\Omega\xi\tau)\bar{\omega}}{\dfrac{8\vartheta+12\vartheta\Omega\xi\tau}{(1-\hat{w}_{\text{tip}})^2} + \dfrac{3}{(1-\hat{w}_{\text{tip}})^2} + \dfrac{1.95k}{(1-\hat{w}_{\text{tip}})}} & \text{nanobeam} \\ \dfrac{24\hat{w}_{\text{tip}}(1+\delta) - \dfrac{8\gamma\vartheta+12\vartheta\gamma\Omega\xi\tau}{(1-\hat{w}_{\text{tip}})^4} - \dfrac{15k^{\frac{1}{2}}\gamma}{16(1-\hat{w}_{\text{tip}})^{\frac{7}{2}}} - 8\vartheta\bar{\omega} - 12\vartheta\Omega\xi\tau\bar{\omega} - \dfrac{3\bar{\omega}}{4}}{\dfrac{6\bar{k}^{\frac{3}{2}}}{\sqrt{(1-\hat{w}_{\text{tip}})[1+\bar{k}(1-\hat{w}_{tip})]}\operatorname{arccosh}^2(1+2\bar{k}(1-\hat{w}_{\text{tip}}))} + \dfrac{8\vartheta+12\vartheta\Omega\xi\tau}{(1-\hat{w}_{\text{tip}})^2}} & \text{nanowire} \end{cases} \tag{34}$$

The pull-in parameters of the sensors can be obtained from Eqs. (34) by setting $d\beta/d\hat{w}_{tip} = 0$.

4 Results and Discussion

4.1 Validation

To examine the accuracy of the theoretical model the obtained results are compared with the experiment and COMSOL simulation data (Qian et al. 2012). Qian et al. measured the pull-in voltage of the U-shaped NEMS made of silicon nanobeams (Qian et al. 2012). Their NEMS consists of a capacitive rigid plate with 2 μm length and 4 μm width supported by two nearly square cross-section nanobeams with 5 μm length and 145 nm initial gap. Table 1 presents a comparison between the present theoretical model and those of experiments and COMSOL simulation (Qian et al. 2012). As seen, a good agreement is observed between the proposed model and those of experiments and simulation. This implies the reliability of the present model in determining the instability voltage of the systems.

Table 1 Pull-in voltage comparison between the proposed solution and experimental reports (Qian et al. 2012)

Case	Experiment (Qian et al. 2012)	COMSOL (Qian et al. 2012)	RRM
Pull-in voltage (V)	1.12	1.04	1.034
Error* (%)	–	7.1	7.7

* Relative with experiment

4.2 Results

The deflection of U-shaped sensor as a function of applied voltage is demonstrated in Fig. 3. As seen from this figure,

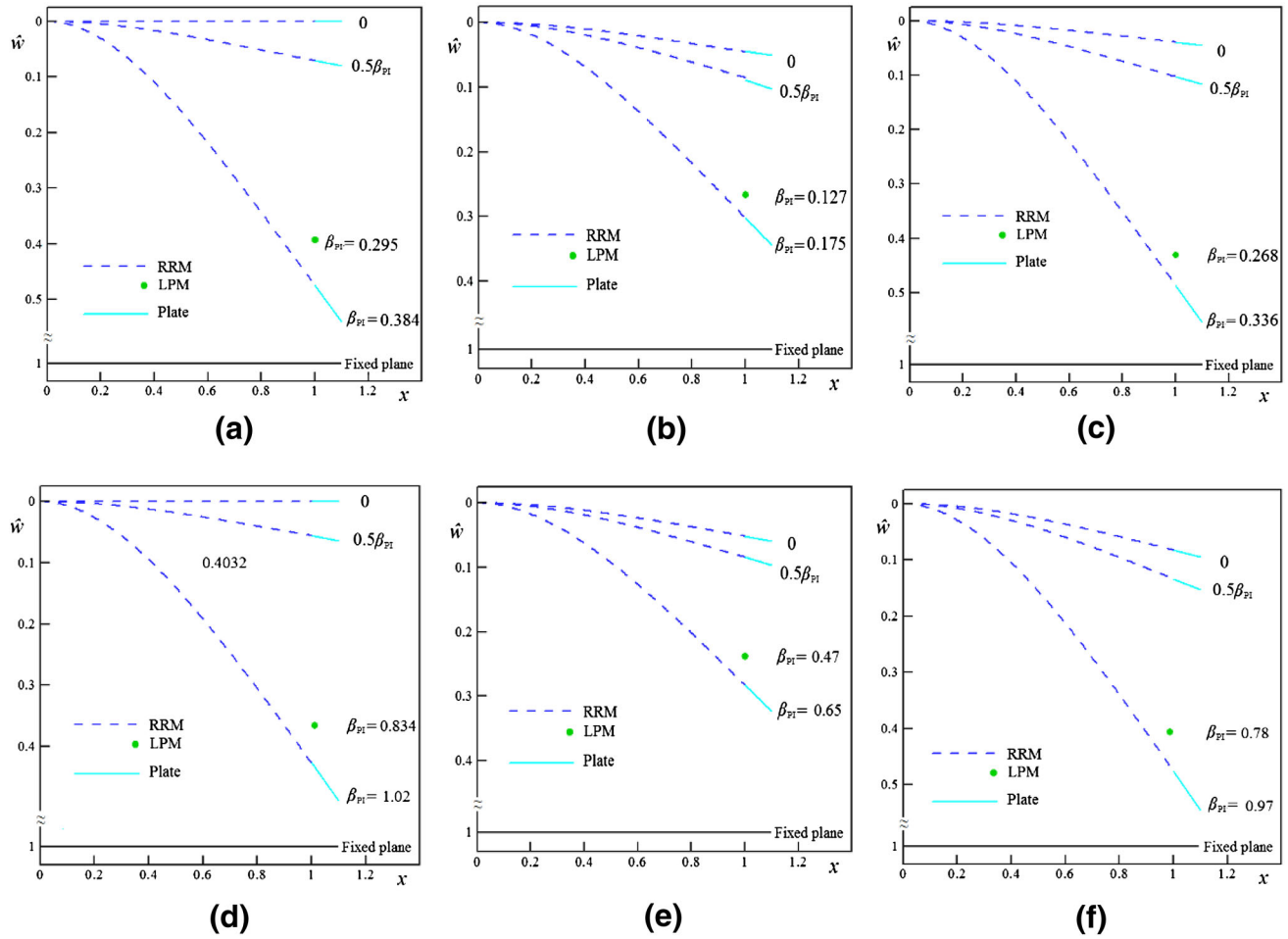

Fig. 3 Tip displacement variation of the U-shape sensor for different values of β ($k = 6$, $\xi = 0.5$, $\tau = 0.2$, $\vartheta = 0.2$, $\Omega = 0.5$ and $\delta = 0$); **a** nanobeam, neglecting the Casimir and centrifugal forces, **b** nanobeam, considering Casimir force and no centrifugal force ($\gamma = 0.2$, $\bar{\omega} = 0$), **c** nanobeam, considering centrifugal force and no Casimir force ($\gamma = 0.0$, $\bar{\omega} = 0.2$), **d** nanowire, neglecting the Casimir and centrifugal forces, **e** nanowire, considering Casimir force and no centrifugal force ($\gamma = 0.2$, $\bar{\omega} = 0$), **f** nanowire, considering centrifugal force and no Casimir force ($\gamma = 0.0$, $\bar{\omega} = 0.2$)

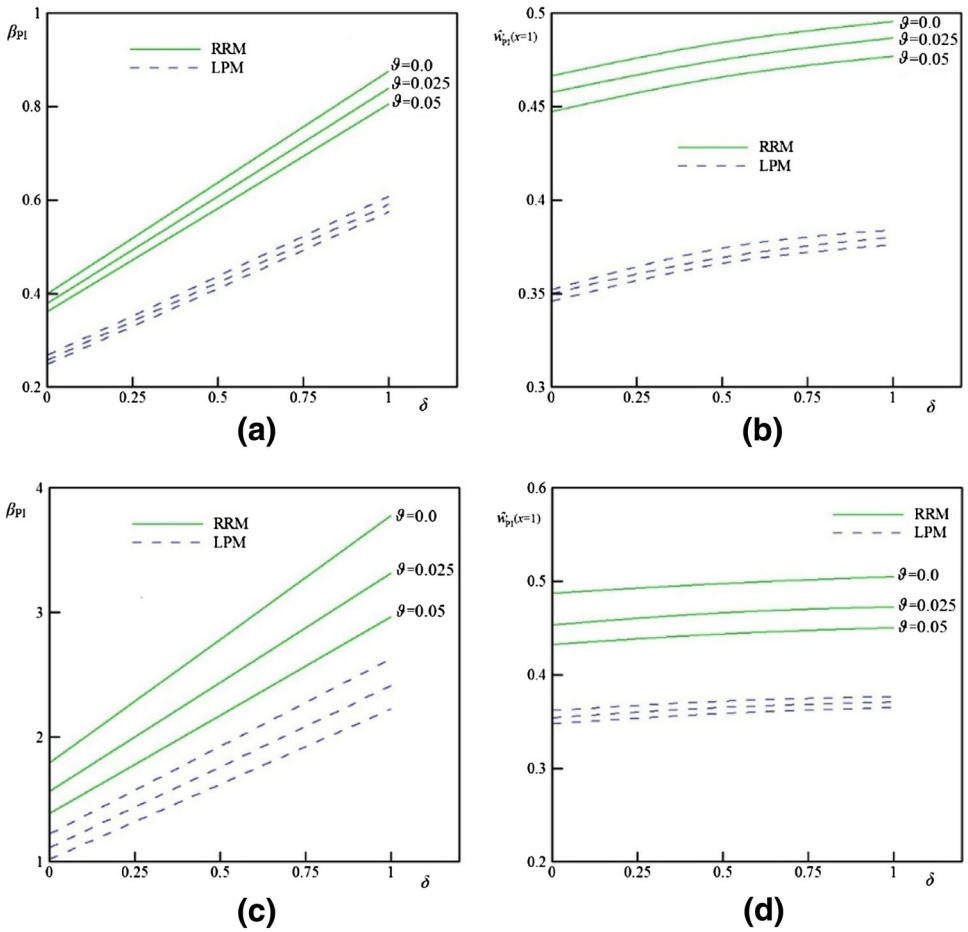

Fig. 4 The variation of the β_{PI} and $\hat{w}_{PI}$ $(x = 1)$ versus δ for different values of ϑ $(k = 6, \xi = 0.25, \tau = 0.1, \Omega = 0.5, \bar{\omega} = 0$ and $\gamma = 0.1)$; **a** nanobeam, β_{PI} **b** nanobeam, $\hat{w}_{PI}$ $(x = 1)$ **c** nanowire, β_{PI} **d** nanowire, $\hat{w}_{PI}$ $(x = 1)$

increasing the dimensionless voltage (β) leads to an increase in the deflection. Figure 3a, d show the variation of the beam/wire deflection in the absence of the Casimir and centrifugal forces ($\gamma = \bar{\omega} = 0$). Figure 3b, e demonstrate the bending of the sensors in the presence of the Casimir force without any centrifugal force ($\gamma = 0.2$, $\bar{\omega} = 0$). Figure 3c, f illustrate the deflection of the sensors by ignoring the Casimir force and considering a positive value of the centrifugal force ($\gamma = 0$, $\bar{\omega} = 0.2$). As shown in these figures, a positive value of the centrifugal force reduces the instability voltage while slightly enhances the pull-in deflection of the system. Moreover, these figures reveal that both pull-in voltage and pull-in deflection are reduced in the presence of the Casimir force.

Figure 4 shows the effects of the scale-dependency on the instability parameters of the system. The size phenomenon should be taken into account for precise modeling of the sensors made of size-dependent materials such as metals (Lam et al. 2003; McFarland and Colton 2005). The zero value of δ denote the classic continuum theory results. This figure reveals that the pull-in characteristics enhance by increasing the size parameter (δ). Figure 4 demonstrates that by considering the size dependency (for $\delta = 1$) the pull-in voltage of nanobeam based on the CCST is 2.2 times greater than classical results. Similarly, the size-dependent theory predicts the pull-in voltage of nanowire 2.1 times greater than classical theory. A comparison between Fig. 4b, d demonstrates that while the size dependency don't change the pull-in deflection of nanowire significantly (2.8%), the CCST leads to a 6.6% increase in the pull-in deflection of nanobeam.

Figure 5 examine the impact of centrifugal force on the pull-in voltage of the sensor. This figure reveals that for positive values of centrifugal force, the pull-in voltage reduces by enhancing the angular speed. In contrast, the pull-in voltage grows up by increasing the angular velocity when negative centrifugal force is applied. Figure 5 demonstrates that the centrifugal force change the pull-in parameters of nanobeam more significantly than the pull-in characteristic of nanowire.

The critical values of centrifugal force, $\bar{\omega}_{cr}$, can be acquired by setting $\beta = 0$ and then solving the governing equation. For $\bar{\omega}$ greater than critical value of centrifugal force ($\bar{\omega}_{cr} > \bar{\omega}_{cr}$), stiction occurs and no solution exists. The maximum allowed length of the beam/wire L_{max}, to avoid the stiction is a critical parameter in NEMS design

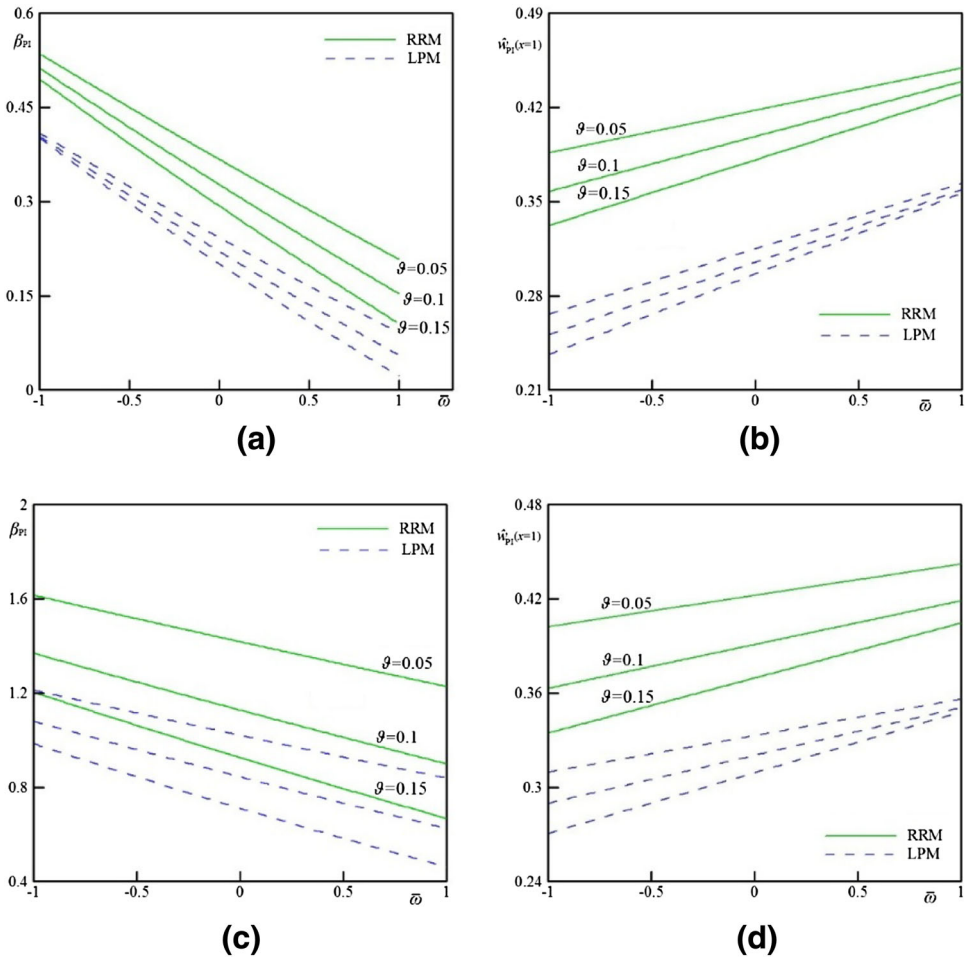

Fig. 5 The variation of β_{PI} and $\hat{w}_{PI}$ $(x = 1)$ versus $\bar{\omega}$ for different values of ϑ ($k = 5$, $\xi = 0.25$, $\tau = 0.25$, $\Omega = 0.5$, $\delta = 0$ and $\gamma = 0.15$); **a** nanobeam, β_{PI} **b** nanobeam, $\hat{w}_{PI}$ $(x = 1)$ **c** nanowire, β_{PI} **d** nanowire, $\hat{w}_{PI}$ $(x = 1)$

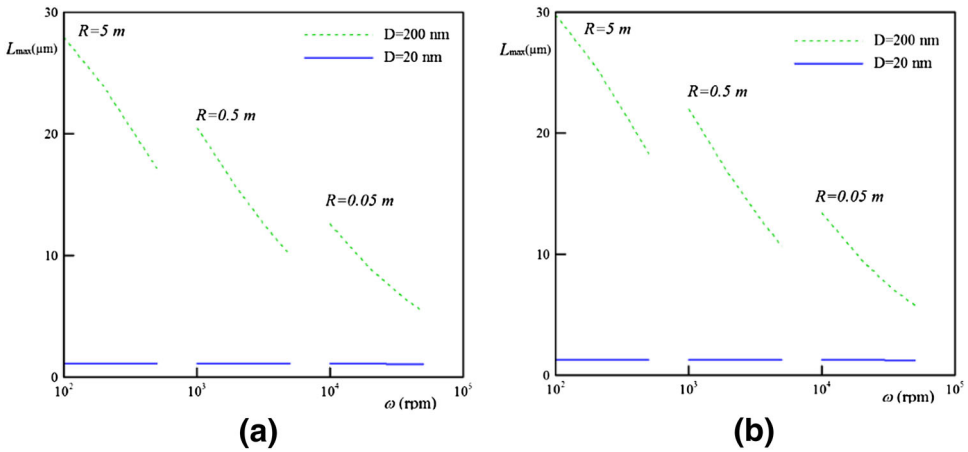

Fig. 6 Variation of the L_{max} as a function of the R and ω in the presence of centrifugal force ($\bar{\omega} \neq 0$) for typical gold U-shaped sensors ($E = 80$ GPa, $\rho = 19.3$ g/cm^3, $\delta = 0$, $a = 1000$ nm and $b = 1000$ nm); **a** nanobeam **b** nanowire

and fabrication (Lin and Zhao 2005). The value of L_{max} can be determined by determining $\bar{\omega}_{cr}$ (considering $\beta = 0$ and solving Eq. (25), and then substituting $\bar{\omega}_{cr}$ into the definition of $\bar{\omega}$ (Eq. 25). The L_{max} variation as a function of the R and ω is illustrated in Fig. 6. The values of $R = 5$ cm, $R = 0.5$ m and $R = 5$ m are for the radii of typical centrifuge rotor, airplane propeller and helicopter blade, respectively. The rigid plate has the length of 1 μm and width of 1 μm. As shown in this figure, it can be said that for small separation ($D = 20$ nm), the ω value does not substantially affect the L_{max} of the beam/wire; while, at larger distances ($D = 200$ nm), increasing the ω value leads to significant reduce in L_{max} of the beam/wire. Moreover, increasing the angular speed decreases the L_{max}.

5 Conclusions

Herein, the influence of centrifugal force on the instability behavior of U-shaped sensor operated in Casimir regime is investigated. A size dependent model based on the CCST was developed to incorporate the size phenomenon on the governing equation of each nanostructure. The constitutive equations are solved using two different solution methods. The obtained results reveal that for positive values of the centrifugal force, the pull-in voltage decreases as the angular speed increases. On the other hand, for negative values of the centrifugal force, an increase in the angular velocity increases the stability threshold of these systems. The variation of the detachment length of the freestanding sensors as a function of the centrifugal force was determined. While the Casimir force reduces the instability threshold, the pull-in voltage is increased by enhancing the size parameter. The pull-in characteristics and the critical value of Casimir force were significantly affected by geometrical characteristics of the structures. The results of presented model are in good agreement with those of literature. While less precise results can be provided using LPM, however, this model simply explains the instability behavior without mathematical complexity. The obtained results are beneficial to design and fabrication of U-shaped systems.

References

Abdi J, Koochi A, Kazemi AS, Abadyan M (2011) Modeling the effects of size dependence and dispersion forces on the pull-in instability of electrostatic cantilever NEMS using modified couple stress theory. Smart Mater Struct 20(5):055011

Azimloo H, Rezazadeh G, Shabani R, Sheikhlou M (2014) Bifurcation analysis of an electro-statically actuated micro-beam in the presence of centrifugal forces. Int J Nonlinear Mech 67:7–15

Baghani M (2012) Analytical study on size-dependent static pull-in voltage of microcantilevers using the modified couple stress theory. Int J Eng Sci 54:99–105

Bodson M, Chiasson J, Novotnak RT (1995) Nonlinear speed observer for high-performance induction motor control. Ind Electron IEEE Trans 42(4):337–343

Bordag M, Mohideen U, Mostepanenko VM (2001) New developments in the Casimir effect. Phys Rep 353(1):1–205

Ejike U (1969) The plane circular crack problem in the linearized couple-stress theory. Int J Eng Sci 7:947–961

Emig T, Jaffe RL, Kardar M, Scardicchio A (2006) Casimir interaction between a plate and a cylinder. Phys Rev Lett 96(8):080403

Eringen AC, Edelen DGB (1972) On nonlocal elasticity. Int J Eng Sci 10(3):233–248

Fakhrabadi MMS, Yang J (2015) Comprehensive nonlinear electromechanical analysis of nanobeams under DC/AC voltages based on consistent couple-stress theory. Compos Struct 132:1206–1218

Farrokhabadi A, Mokhtari J, Rach R, Abadyan M (2015a) Modeling the influence of the Casimir force on the pull-in instability of nanowire-fabricated nanotweezers. Int J Mod Phys B 29(02):1450245

Farrokhabadi A, Mokhtari J, Koochi A, Abadyan M (2015b) A theoretical model for investigating the effect of vacuum fluctuations on the electromechanical stability of nanotweezers. Indian J Phys 89(6):599–609

Gupta RK (1997) Electrostatic pull-in test structure design for in situ mechanical property measurements of microelectromechanical systems. PhD Dissertation Massachusetts Institute of Technology (MIT), Cambridge, MA

Hadjesfandiari AR, Dargush GF (2011) Couple stress theory for solids. Int J Solids Struct 48(18):2496–2510

Hayt WH (1981) Engineering electromagnetics. McGraw-Hill, New York

Hou C, Wu Y, Zeng X, Zhao S, Zhou Q, Yang G (2010) Novel high sensitivity accelerometer based on a microfiber loop resonator. Opt Eng 49(1):014402

Huang CT, Li PN, Pai CY, Leu TS, Jen CP (2009) Design and simulation of a microfluidic blood-plasma separation chip using microchannel structures. Sep Sci Technol 45(1):42–49

Jackson JD (1998) Classical electrodynamics. Wiley, New York

Jywe WY, Chen CJ (2005) The development of a high-speed spindle measurement system using a laser diode and a quadrants sensor. Int J Mach Tools Manuf 45(10):1162–1170

Ke CH, Espinosa HD (2006) Nanoelectromechanical systems (NEMS) and modeling. Handbook of Theoretical and Computational Nanotechnology, American Scientific Publishers, Valencia

Keivani M, Khorsandi J, Mokhtari J, Kanani A, Abadian N, Abadyan M (2016a) Pull-in instability of paddle-type and double-sided NEMS sensors under the accelerating force. Acta Astronaut 119:196–206

Keivani M, Kanani A, Mardaneh MR, Mokhtari J, Abadyan N, Abadyan M (2016b) Influence of accelerating force on the electromechanical instability of paddle-type and double-sided sensors made of nanowires. Int J Appl Mech 8(01):1650011

Keivani M, Koochi A, Abadyan M (2016c) A new model for stability analysis of electromechanical nano-actuator based on Gurtin-Murdoch and consistent couple-stress theories. J VibroEng 18(3):1406–1416

Keivani M, Gheisari R, Kanani A, Abadian N, Mokhtari J, Rach R, Abadyan M (2016d) Effect of the centrifugal force on the electromechanical instability of U-shaped and double-sided sensors made of cylindrical nanowires. J Braz Soc Mech Sci Eng 38(7):2129–2148

Keivani M, Abadian N, Koochi A, Mokhtari J, Abadyan M (2016e) A 2-DOF microstructure-dependent model for the coupled torsion/bending instability of rotational nanoscanner. Appl Phys A 122(10):927

Keplinger F, Beigelbeck R, Kohl F, Kvasnica S, Jachimowicz A, Jakoby B (2005) Frequency and transient analysis of micromachined U-shaped cantilever devices for magnetic field measurement. Poster: 13th European Conference on Solid-State Sensors Actuators and Microsystems, Seoul, Korea; 06-05-2005–06-09-2005; in: "Digest of Technical Papers" ISBN: 0-7803-8994-8; 630–635

Kopka P, Hoffmann M, Voges E (2000) Coupled U-shaped cantilever actuators for 1×4 and 2×2 optical fibre switches. J Micromech Microeng 10(2):260

Koukharenko E, Beeby SP, Tudor MJ, White NM, O'Donnell T, Saha C, Kulkarni C, Roy S (2006) Microelectromechanical systems vibration powered electromagnetic generator for wireless sensor applications. Microsyst Technol 12(10–11):1071–1077

Lam DCC, Yang F, Chong ACM, Wang J, Tong P (2003) Experiments and theory in strain gradient elasticity. J Mech Phys Solids 51(8):1477–1508

Latorre L, Nouet P, Bertrand Y, Hazard P, Pressecq F (1999) Characterization and modeling of a CMOS-compatible MEMS technology. Sensors Actuators A: Phys 74(1):143–147

Lebold MS, Maynard K, Reichard K, Trethewey M, Bieryla D, Lissenden C, Dobbins D (2004) Using torsional vibration analysis as a synergistic method for crack detection in rotating equipment. In: Aerospace conference, proceedings 2004 IEEE (Vol 6, pp 3517–3527)

Lee KB (2007) Closed-form solutions of the parallel plate problem. Sens Actuators A: Phys 133(2):518–525

Lin WH, Zhao YP (2005a) Nonlinear behavior for nanoscale electrostatic actuators with Casimir force. Chaos, Solitons Fractals 23(5):1777–1785

Lin WH, Zhao YP (2005b) Casimir effect on the pull-in parameters of nanometer switches. Microsyst Technol 11(2–3):80–85

Lin WH, Zhao YP (2008) Pull-in instability of micro-switch actuators: model review. Int J Nonlinear Sci Numer Simul 9(2):175–184

McFarland AW, Colton JS (2005) Role of material microstructure in plate stiffness with relevance to microcantilever sensors. J Micromech Microeng 15(5):1060

Mokhtari J, Farrokhabadi A, Rach R, Abadyan M (2015) Theoretical modeling of the effect of Casimir attraction on the electrostatic instability of nanowire-fabricated actuators. Phys E: Low-dimension Syst Nanostruct 68:149–158

Mouloodi S, Khojasteh J, Salehi M, Mohebbi S (2014) Size dependent free vibration analysis of multicrystalline nanoplates by considering surface effects as well as interface region. Int J Mech Sci 85:160–167

Qian Y, Lou L, Tsai MJ, Lee C (2012) A dual-silicon-nanowires based U-shape nanoelectromechanical switch with low pull-in voltage. Appl Phys Lett 100(11):113102

Renaudin L, Bonnardot F, Musy O, Doray JB, Rémond D (2010) Natural roller bearing fault detection by angular measurement of true instantaneous angular speed. Mech Syst Signal Process 24(7):1998–2011

Rezazadeh M, Tahani M, Hosseini SM (2015) Thermoelastic damping in a nonlocal nano-beam resonator as NEMS based on the type III of Green-Naghdi theory (with energy dissipation). Int J Mech Sci 92:304–311

Shah-Mohammadi-Azar A, Azimloo H, Rezazadeh G, Shabani R, Tousi B (2013) On the modeling of a capacitive angular speed measurement sensor. Measurement 46(10):3976–3981

Yan D, Khajepour A, Mansour R (2004) Design and modeling of a MEMS bidirectional vertical thermal actuator. J Micromech Microeng 14(7):841

Yang FACM, Chong ACM, Lam DCC, Tong P (2002) Couple stress based strain gradient theory for elasticity. Int J Solids Struct 39(10):2731–2743

Zhang J, Fu Y (2012) Pull-in analysis of electrically actuated viscoelastic microbeams based on a modified couple stress theory. Meccanica 47(7):1649–1658

Zhu HX (2010) Size-dependent elastic properties of micro-and nano-honeycombs. J Mech Phys Solids 58(5):696–709